Tree-ring cellulose oxygen isotope reveals summer hydroclimate variability across the East European Plain

Qiaoyun Lin[1, 2], Chenxi Xu[1, 2, *], Ru Huang[1, 3], Wenling An[1, *], Vladimir Matskovsky[4], Olga Solomina[4, 5], Ekaterina Dolgova[4], Yaru Zhao[1], Zhengtang Guo[1, 2]

[1] State Key Laboratory of Lithospheric and Environmental Coevolution, Institute of Geology and Geophysics, Chinese Academy of Sciences, Beijing 100029, China

[2] College of Earth and Planetary Sciences, University of Chinese Academy of Sciences, Beijing 100049, China

[3] Department of Environment and Biodiversity, University of Salzburg, Salzburg, 5020, Austria

[4] Institute of Geography RAS, Moscow, Russia

[5] HSE University, Moscow, Russia

Correspondence to: Chenxi Xu (cxxu@mail.iggcas.ac.cn); Wenling An (wlan@mail.iggcas.ac.cn)

Abstract. Hydroclimate variability across the East European Plain plays a critical role in regional ecosystems and climate dynamics, yet moisture-sensitive tree-ring proxies remain scarce in this region, particularly at high latitudes where tree-ring width (TRW) and density are primarily controlled by temperature. Tree-ring cellulose oxygen isotopes ($\delta^{18}O_{TRC}$) have the potential to serve as a useful hydroclimate proxy, but their climatic signal in this region remain poorly understood. Here, we developed three $\delta^{18}O_{TRC}$ chronologies of Scots pine (*Pinus sylvestris* L.) from the northern, central, and southern East European Plain to assess their climate signals. The $\delta^{18}O_{TRC}$ chronologies from the three sites show similar response to summer moisture condition. The northern $\delta^{18}O_{TRC}$ shows the strongest relationship with vapor pressure deficit (VPD), the central $\delta^{18}O_{TRC}$ records both hydroclimate variability and precipitation oxygen isotopes ($\delta^{18}O_p$) signals, and the southern $\delta^{18}O_{TRC}$ mainly reflects the Standardized Precipitation Evapotranspiration Index (SPEI). In contrast, TRW shows weak hydroclimate sensitivity at the northern and central sites, whereas at the southern site it mainly reflects soil moisture. Overall, compared with TRW, $\delta^{18}O_{TRC}$ better captures regional summer hydroclimate signals, particularly capturing signals related to atmospheric drought.

Keywords: East European Plain, *Pinus sylvestris* L., Tree-ring cellulose oxygen isotopes, Hydroclimate

1 Introduction

East European Plain occupies a pivotal position in the Eurasian climate system, serving as a key transitional region between the North Atlantic, Europe, and the continental interior of Asia (Liu et al., 2014; Morozova et al., 2023). Understanding climate variability in this region is fundamental for interpreting large-scale climate variability across Eurasia. With global warming, this region has experienced pronounced temperature increases accompanied by complex and spatially heterogeneous changes in hydroclimate (Moberg et al., 2006; Spinoni et al., 2015; Zolina et al., 2009). Historical analyses of hydroclimate variability over past centuries using proxy data are an essential quantitative way to put current conditions in a longer-term perspective.

Tree-ring proxies have been widely used to reconstruct past climate because they are broadly distributed, long-lived, annually resolved, and climate-sensitive (McCarroll and Loader, 2004). To date,

tree-ring width (TRW)-based climate-signal studies in the East European Plain span from the Arctic margin to the southern Caucasus (Solomina and Matskovsky, 2021). However, the application of TRW to climate reconstructions in this region remains limited. First, TRW–climate relationships show pronounced regional differences across the East European Plain, with a transition from temperature limitation to moisture limitation around 55–60° N (Matskovsky, 2016). North of approximately 60° N, conifer TRW generally responds positively to summer temperature, with the strongest responses occurring mainly in June and July (Dolgova et al., 2022; Matskovsky, 2016; Semenyak and Dolgova, 2023). In the central transitional region at approximately 54–56° N, TRW is jointly influenced by summer temperature and moisture conditions, with the main moisture-related variables including precipitation, PDSI, and soil moisture (Matskovsky, 2016). Farther south, in the southern Middle Volga region and the forest-steppe zone of Voronezh, pine growth is primarily limited by warm-season moisture availability (Kuznetsova and Solomina, 2022; Matveev et al., 2019).

Second, TRW at most sites shows low-to-moderate climate sensitivity (correlation coefficients rarely exceed 0.5) (Hughes et al., 2019; Solomina and Matskovsky, 2021). Consequently, although TRW has been used to reconstruct past hydroclimate variability, moisture-sensitive sites capable of capturing interannual hydroclimate variability remain scarce and unevenly distributed, particularly at high latitudes (Cook et al., 2020; Kuznetsova and Solomina, 2022; Matskovsky et al., 2017). This motivates us to explore alternative hydroclimate proxies with more directly process-based interpretations and stronger moisture sensitivity.

Compared with TRW, tree-ring cellulose oxygen isotope ($\delta^{18}O_{TRC}$) typically shows lower within-tree variability, higher inter-tree coherence, and no or very limited age-related effects, making it a widely utilized hydroclimate proxy over the globe (Rinne, 2012; Römer et al., 2025; Xu et al., 2011). $\delta^{18}O_{TRC}$ is mainly controlled by (i) the isotopic composition of source water ($\delta^{18}O_s$), which largely reflects precipitation oxygen isotopes ($\delta^{18}O_p$), (ii) evaporative enrichment of leaf water, and (iii) oxygen exchange with xylem water during cellulose formation (McCarroll and Loader, 2004; Roden et al., 2000). These processes are modulated by factors such as temperature, precipitation amount, moisture-transport history, relative humidity (RH), and wind speed (Gat, 1996; Roden et al., 2000). Consequently, $\delta^{18}O_{TRC}$ can preserve climate information from seasonal to interannual timescales and can be used to reconstruct multiple hydroclimate variables, including precipitation (Rinne, 2012; Xu et al., 2023), RH (Haupt et al., 2011), vapor pressure deficit (VPD) (Nagavciuc et al., 2024; Treydte et al., 2024), and drought indices

(An et al., 2023; Arosio et al., 2025; Freund et al., 2023; Xu et al., 2013a).

Although networks of tree-ring $\delta^{18}O$ chronologies have been widely developed across Europe and Asia and applied to hydroclimate reconstructions (Freund et al., 2023; Treydte et al., 2024; Xu et al., 2024), the climate sensitivity of $\delta^{18}O_{TRC}$ shows pronounced regional variability. Moisture sources and transport pathways influence the isotopic composition of precipitation and tree source water, whereas local relative humidity and evaporative demand regulate leaf-water evaporative enrichment (Gat, 1996; McCarroll and Loader, 2004; Roden et al., 2000). Soil-water storage and seasonal mixing can further alter the contribution of precipitation from different seasons to tree source water, potentially extending the $\delta^{18}O$ climate response beyond the period of cellulose formation (Treydte et al., 2014). Consequently, the dominant controls, response strength, and seasonal response windows of $\delta^{18}O_{TRC}$ may differ among hydroclimatic settings (Freund et al., 2023; Treydte et al., 2007). This spatial heterogeneity highlights the need for region-specific studies of climate signals. In contrast, tree-ring isotope research in the East European Plain is limited (Matskovsky et al., 2022; Panyushkina et al., 2016), and the ability of $\delta^{18}O_{TRC}$ to capture interannual hydroclimate variability in this region remains a significant knowledge gap.

Given the pronounced north–south gradients and spatial heterogeneity in interannual variability and long-term trends of temperature and precipitation (Klimenko and Solomina, 2010), a single site cannot adequately represent the regional-scale climate sensitivity of $\delta^{18}O_{TRC}$. Here, we sampled Scots pine (*Pinus sylvestris* L.) from three representative forest regions in the northern, central, and southern East European Plain (51–65° N) and developed site-level $\delta^{18}O_{TRC}$ chronologies along this transect. Our objectives were to (1) quantify the relative contributions of $\delta^{18}O_p$ and RH-related evaporative enrichment to the spatial difference in $\delta^{18}O_{TRC}$; (2) identify the dominant climate signal and key seasonal windows of $\delta^{18}O_{TRC}$ at the interannual scale; and (3) evaluate the potential of $\delta^{18}O_{TRC}$ for reconstructing historical hydroclimate variability in the East European Plain.

2 Material and methods

2.1 Study area

The study area is located in the East European Plain and is characterized by cold winters, warm summers, and pronounced seasonality. The relatively flat topography of the East European Plain, together with the low relief of Central and Western Europe, allows Atlantic moisture carried by the prevailing

westerlies to penetrate far inland toward the Ural Mountains (Klimenko and Solomina, 2010).

The geographic locations of the three sampling sites are shown in Fig. 1a and Table 1. The northern sampling site is located on the Solovetsky Islands, which have a subarctic climate. Owing to the maritime influence of the White Sea, the islands experience milder temperatures, smaller diurnal temperature ranges, higher humidity, and stronger winds than the adjacent mainland coast (Semenyak and Dolgova, 2023). The central sampling site is located in Yaroslavl city and has a temperate continental climate. The surrounding forests are mainly coniferous and dominated by Scots pine. The site lies within a forest park in an urban zone and may be influenced by anthropogenic disturbance. The southern sampling site is located in Khrenovskoy Forest (Voronezh Oblast) and has a temperate continental climate. The forest lies in the forest-steppe zone and represents the southernmost natural pine forest in the East European Plain (Matskovsky et al., 2017), with Scots pine as the dominant tree species (Matveev et al., 2017).

From 1950–2021 (precipitation for the central site is only available for 1967–2021; Fig. 1b–d), mean annual precipitation was 480, 623, and 489 mm at the northern, central, and southern sites, respectively. Mean annual temperatures were 1.52, 3.85, and 6.51 °C, respectively. Mean summer (June–August) temperature increased from 12.86 °C at the northern site to 16.73 °C at the central site and 19.66 °C at the southern site. The lowest mean RH occurred in June at the northern site (69.54 %) and in May at the central (63.56 %) and southern (56.71 %) sites (Fig. 1b–d).

Scots pine was selected as the study species. It is long-lived (up to ~400 years) and widely distributed across northern Eurasia (Lange et al., 2018). Xylogenesis observations indicate pronounced latitudinal differences in growth phenology: in northern insular ecosystems near our northern site, growth typically begins in early June and ceases by mid to late August, whereas at more southerly sites xylem formation generally starts earlier (from late April to May) and ends later (from late August to September) (Matulewski et al., 2019; Matveev et al., 2020; Tishin et al., 2016).

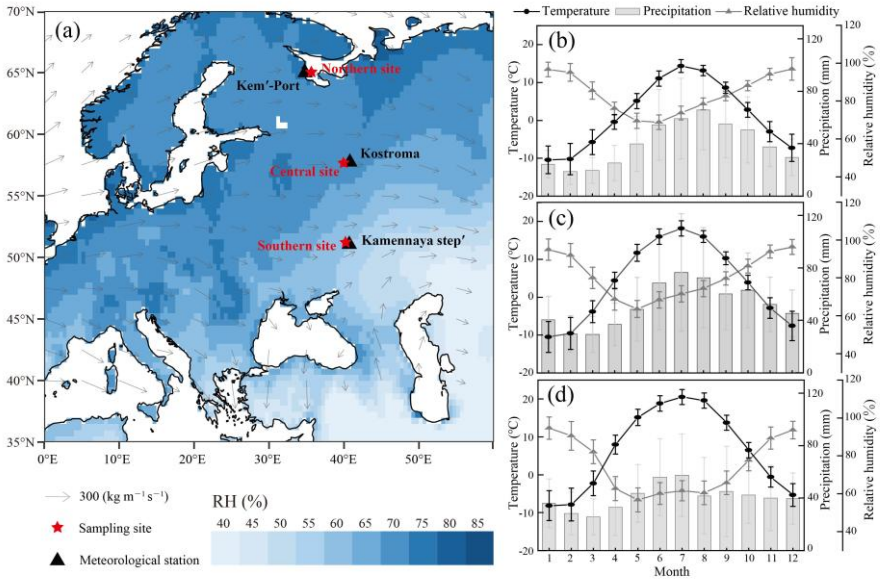


Figure 1. Study site locations and climatic characteristics. (a) Arrows indicate the mean vertically integrated water vapor flux (kg m^{-1} s^{-1}) and the transport direction for May to September, 1950–2019. (b–d) show mean monthly temperature, precipitation, and RH at the northern, central, and southern sites, respectively. Temperature and precipitation data were obtained from meteorological stations, whereas RH was calculated from CRU TS 4.08 gridded temperature and vapor pressure (Harris et al., 2020). All mean monthly values are for 1950–2021, except for central-site precipitation (1967–2021).

Table 1. Location, environmental characteristics, and $\delta^{18}O_{TRC}$ chronology statistics.

Site	Latitude (° N)	Longitude (° E)	Elevation (m)	Mean $\delta^{18}O_{TRC}$ (‰)	SD (‰)	AC1	Rbar	EPS	Age (yr)
N	65.039	35.641	9m	26.36	0.60	–0.09	0.67	0.89	1950–2021
C	57.647	39.932	110m	27.61	0.61	0.15	0.57	0.84	1950–2020
S	51.201	40.199	94m	30.52	0.68	0.13	0.58	0.84	1950–2014

N, C, S denote northern, central, southern sites, respectively. SD, AC1, Rbar, and EPS represent the standard deviation, first-order autocorrelation, mean interseries correlation, and expressed population signal, respectively.

2.2 Sampling, Sample Preparation and Isotope Analysis

Initially, the cores were collected for dendroclimatic analysis at breast height using increment corers from dominant and subdominant trees. The cores were mounted on wooden bases with polyvinyl alcohol (PVA) glue, polished, and scanned. Tree-ring widths (TRW) were measured in CooRecorder, and cross-

dating was verified for all samples using COFECHA (Holmes, 1983). The TRW chronologies used in this study were developed by detrending and standardizing the ring-width series with the ARSTAN program. Previous analyses of TRW data from these sites are available in Dolgova et al. (2022) and Semenyak and Dolgova (2023).

The numbers of candidate samples and the results of core selection for $\delta^{18}O_{TRC}$ analysis are summarized in Table S1. The same selection criteria were applied at all three sites, including preferentially selecting the oldest cores to minimize potential juvenile effects, reliable cross-dating and continuous temporal coverage, clearly identifiable ring boundaries, and the ability to isolate individual rings without contamination from adjacent rings while obtaining sufficient α-cellulose for isotope measurement (Xu et al., 2011, 2013b). Narrow rings were retained as long as they could be reliably separated and provided sufficient material, whereas cores containing missing rings or rings that could not be reliably separated and measured were not selected. Based on these criteria, four cores from four different trees were initially selected from all candidate cores at each site. Additional sampling at the northern site in 2021 provided three further cores covering 2000–2021, allowing the isotope chronology to be extended to 2021.α-cellulose was extracted using a modified plate method (Xu et al., 2011, 2013b). Cores were cut into ~1 mm thick, and ~7 cm long slivers and processed following the Jayme–Wise protocol (Loader et al., 1997). Specifically, lignin, hemicellulose, and lipids were sequentially removed by treatment with acidified $NaClO_2$, 17 wt% NaOH, and organic solvents (acetone, toluene, and ethanol), respectively. After chemical treatment, the α-cellulose slivers were oven-dried at 70 °C. Annual α-cellulose subsamples were separated under a binocular microscope using a scalpel. The α-cellulose samples (0.12–0.20 mg) were weighed and wrapped in silver foil for oxygen isotope analysis.

$\delta^{18}O_{TRC}$ values were measured at the Institute of Geology and Geophysics, Chinese Academy of Sciences, using an isotope ratio mass spectrometer (Delta V Advantage, Thermo Scientific, Germany) coupled to a high-temperature conversion elemental analyzer (Flash HT, Thermo Scientific, Germany). Oxygen isotope ratios are reported in δ notation relative to Vienna Standard Mean Ocean Water (VSMOW): $\delta^{18}O = [(R_{sample}/R_{standard}) - 1] \times 1000‰$, where R_{sample} and $R_{standard}$ denote the $^{18}O/^{16}O$ ratios of the sample and standard, respectively. For calibration and quality control, a Merck cellulose working standard was analyzed after every eight samples, and $\delta^{18}O$ values were normalized to this standard. The analytical uncertainties for repeated measurements of Merck cellulose were ~ ±0.16‰ (n = 149).

168 **2.3 Climate data**

169 Temperature and precipitation data for the northern, central, and southern sites were obtained from
170 the Kem'-Port Meteorological Station (34.80° E, 64.98° N; WMO No. 22520), Kostroma Meteorological
171 Station (40.78° E, 57.73° N; WMO No. 27333), and Kamennaya Step' Meteorological Station (40.70° E,
172 51.05° N; WMO No. 34139), respectively (Fig. 1a). All meteorological station data were obtained from
173 the Russian Institute of Hydrometeorological Information-World Data Centre (RIHMI-WDC).

174 To examine contemporaneous and lagged relationships between $\delta^{18}O_{TRC}$ and additional climatic
175 variables, we used gridded products from the following archives. These included monthly mean
176 temperature (T_{mean}), maximum temperature (T_{max}), minimum temperature (T_{min}), precipitation (Pre),
177 cloud cover (CC), and vapor pressure (VP) from CRU TS 4.08 at 0.5° × 0.5° spatial resolution for 1950–
178 2021 (Harris et al., 2020); drought indices including the Standardized Precipitation Evapotranspiration
179 Index (SPEI) and the Palmer Drought Severity Index (PDSI)(Dai et al., 2004; Vicente-Serrano et al.,
180 2010b); and soil moisture (SM; 0–10 cm and 0–40 cm) from the Famine Early Warning Systems Network
181 Land Data Assimilation System (FLDAS) at 0.1° × 0.1° resolution (McNally et al., 2017).

182 All gridded datasets were accessed and downloaded via the KNMI Climate Explorer (Trouet and
183 Van Oldenborgh, 2013). For each site, gridded variables were spatially averaged within a 2° × 2° box
184 centered on the sampling coordinates. Monthly T_{mean} and VP were used to calculate RH and VPD
185 following formulae (Allen et al., 1998):

186 $$RH=(VP/e_{sat})\times 100 \quad (1)$$

187 $$e_{sat}=6.108\times\exp(17.27\times T/(T+237.3)) \quad (2)$$

188 $$VPD=e_{sat}-VP \quad (3)$$

189 where e_{sat} is saturated vapor pressure (hPa), and T is mean temperature (°C).

190 Given that $\delta^{18}O_p$ is an important control on $\delta^{18}O_{TRC}$, and that nearby Global Network of Isotopes in
191 Precipitation (GNIP; https://www.iaea.org/zh/fu-wu/wang-luo) records are relatively short, GNIP
192 observations alone are insufficient for long-term analyses. Therefore, we used the isotope-enabled
193 atmospheric general circulation model ECHAM5-wiso to obtain $\delta^{18}O_p$ for our study region. ECHAM5-
194 wiso is an isotope-enabled extension of ECHAM5 in which the stable water isotopologues $H_2{}^{18}O$ and
195 HDO are explicitly simulated within the atmospheric hydrological cycle (Werner et al., 2011). We
196 downloaded model-simulated monthly $\delta^{18}O_p$ (https://doi.pangaea.de/10.1594/PANGAEA.902347) and

extracted time series from the grid cell nearest to each study site for 1958–2013. Previous studies have evaluated ECHAM5-wiso against GNIP observations at the global scale (Werner et al., 2011) and across Europe (Langebroek et al., 2011). Moreover, ECHAM5-wiso successfully reproduced the seasonal phase of $\delta^{18}O_p$ observed at nearby GNIP stations, despite a pronounced station-dependent mean offset, particularly at southern stations with limited GNIP coverage (Fig. S1). Consequently, we primarily used ECHAM5-wiso $\delta^{18}O_p$ simulations to interpret interannual variability in source-water isotopes. The latitude, longitude, and other metadata for the simulated and observed $\delta^{18}O_p$ data are provided in Table S2.

2.4 Statistical analyses

The $\delta^{18}O_{TRC}$ series from all analyzed cores at each site were averaged to generate site-level $\delta^{18}O_{TRC}$ chronologies for the northern, central, and southern sites. We calculated the mean interseries correlation (Rbar) to evaluate inter-core coherence and the expressed population signal (EPS) to assess chronology representativeness (Wigley et al., 1984). Rbar was calculated as the mean of all pairwise Pearson correlations among the four original core series at each site, and EPS was derived from Rbar using a fixed sample replication of N = 4. Because the isotope chronologies span only approximately 65–72 years, Rbar and EPS were calculated over the common period of the four original core series at each site rather than using moving-window analyses. The three additional northern series cover only approximately 2000–2021 and were therefore excluded from these calculations.

To explore the factors controlling the spatial differences in $\delta^{18}O_{TRC}$, we used a simplified mechanistic fractionation framework for $\delta^{18}O_{TRC}$ (Roden et al., 2000):

$$\delta^{18}O_{TRC}=\left(\delta^{18}O_S+\varepsilon_0\right)+\alpha\left(1-f_0\right)(1-h)\left(\varepsilon^*+\varepsilon_k\right) \quad (4)$$

Here, $\delta^{18}O_s$ is the oxygen isotopic composition of source water (approximated by $\delta^{18}O_p$); ε_0 is the net biochemical fractionation term associated with cellulose formation; f_0 is the proportion of exchangeable oxygen during cellulose synthesis (set to 0.42; Sternberg and Ellsworth, 2011); ε^* and ε_k are the equilibrium and kinetic fractionation factors, respectively (set to 9‰ and 29‰, respectively; Allison et al., 1985); h is the relative humidity at the evaporative site in the leaf; and α is a scaling/attenuation factor describing the transfer of the evaporative-enrichment signal to cellulose (set to 1; Allison et al., 1985; Barbour, 2007).

We further defined the evaporative enrichment term, E, as

$$E=\alpha\left(1-f_0\right)(1-h)\left(\varepsilon^*+\varepsilon_k\right) \quad (5)$$

Here, Δ denotes the pairwise difference between sites. We then calculated $\Delta\delta^{18}O_{TRC}$, $\Delta\delta^{18}O_p$, ΔRH, and ΔE to quantify the relative contributions of site-to-site differences in $\delta^{18}O_p$ and RH-controlled evaporative enrichment to spatial variability in $\delta^{18}O_{TRC}$.

To identify climatic and source-water signals recorded in $\delta^{18}O_{TRC}$, we correlated the chronology with monthly and seasonal climate variables from June of the previous year to September of the current year, and with $\delta^{18}O_p$ from October of the previous year to September of the current year. Spatial correlations between each site chronology and gridded CRU TS 4.08 data were calculated using the KNMI Climate Explorer (https://climexp.knmi.nl/start.cgi) to evaluate the regional representativeness of $\delta^{18}O_{TRC}$.

3 Results

3.1 Tree-ring cellulose oxygen isotope chronologies

The mean inter-series correlation (Rbar) for the northern $\delta^{18}O_{TRC}$ site was 0.67, and the expressed population signal (EPS) of the chronology was 0.89 (Table 1). By contrast, the central and southern sites showed slightly lower values (Rbar = 0.57 and 0.58, respectively; EPS = 0.84 for both sites; Table 1). Along the north–south transect, the series were averaged to build $\delta^{18}O_{TRC}$ chronologies for the North (1950–2021), Central (1950–2020), and South (1950–2014) (Fig. 2a–d). The original four-tree and expanded seven-tree chronologies at the northern site showed similar interannual variability over their overlapping period (Fig. S2a). EPS was $\geqslant$ 0.84 at all three sites, suggesting overall coherent inter-tree signals within each site. The high within-site inter-series correlations (Table S3) further support the reliability of the $\delta^{18}O_{TRC}$ chronologies.

The northern $\delta^{18}O_{TRC}$ chronology ranged from 24.85‰ to 27.99‰, with a mean of 26.36‰, a standard deviation (SD) of 0.60‰, and a first-order autocorrelation (AC1) of −0.09 (Table 1). The central chronology ranged from 26.23‰ to 28.76‰, with a mean of 27.61‰, an SD of 0.61‰, and an AC1 of 0.15 (Table 1). The southern chronology ranged from 28.93‰ to 31.79‰, with a mean of 30.52‰, an SD of 0.68‰, and an AC1 of 0.13 (Table 1). Over the common period (1950–2014), the northernmost Solovetsky Islands chronology had the lowest median (26.35‰), the central site was 27.62‰, and the southernmost site had the highest median (30.54‰) (Fig. 2e). Overall, both the mean and median values

of the East European Plain $\delta^{18}O_{TRC}$ chronologies show a clear latitudinal gradient, with higher values in the south and lower values in the north.

Pairwise correlations among the three chronologies ranged from 0.14 to 0.35 over 1950–2014. Significant correlations were found for the North–Central pair (NC; r = 0.33, $p < 0.01$) and the Central–South pair (CS; r = 0.35, $p < 0.01$), whereas the North–South pair (NS; r = 0.14, $p > 0.05$) was not significant (Fig. 2e). Overall, these results suggest that $\delta^{18}O_{TRC}$ variability shows local coherence, with stronger similarity between adjacent sites that weakens with increasing distance.

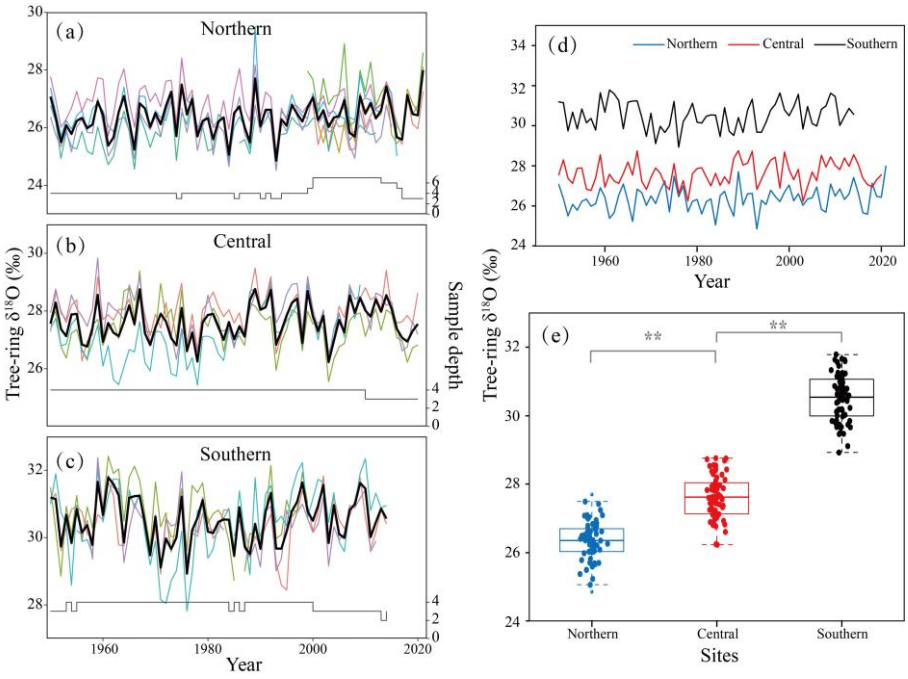


Figure 2. $\delta^{18}O_{TRC}$ chronologies for the northern (a), central (b), and southern (c) East European Plain. Individual $\delta^{18}O_{TRC}$ series are shown as thin colored lines; the site mean chronologies are shown as thick black lines. Annual sample depth is shown by the gray step lines in panels (a–c). Time-series plots (d) and box-and-whisker plots (e; 1950–2014) show the $\delta^{18}O_{TRC}$ chronologies at the three sites. In panel (e), the line within each box denotes the median; box limits indicate the 25th and 75th percentiles; and filled circles denote outliers. Asterisks indicate statistical significance (**, $p < 0.01$).

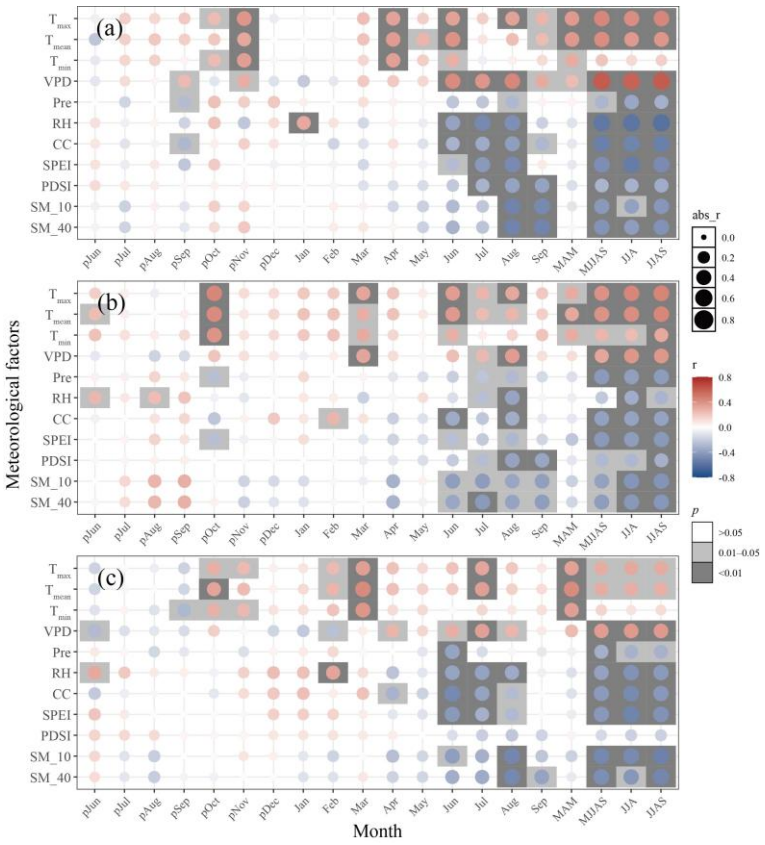
3.2 Climate responses and source water signals of $\delta^{18}O_{TRC}$

During the growing season or summer, $\delta^{18}O_{TRC}$ is significantly positively correlated with VPD, but significantly negatively correlated with moisture-related variables such as Pre, RH, CC, SPEI, PDSI, and SM (Fig. 3; Table S4–S6). Among the three sites, the northern site shows the strongest atmospheric

drying signal, with the highest correlation between $\delta^{18}O_{TRC}$ and May–September VPD ($r = 0.61$, $p < 0.01$, $n = 72$) (Fig. 3; Table S4). In contrast, moisture signals are weaker at the central and southern sites: $\delta^{18}O_{TRC}$ at central site correlates with May–September SPEI at $r = -0.42$ ($p < 0.01$, $n = 69$), whereas the strongest relationship at the southern site is with June–August SPEI ($r = -0.51$, $p < 0.01$, $n = 65$) (Fig. 3; Table S5–S6). By comparison, moisture conditions in the previous year and in spring (March–May) exert relatively limited influence on $\delta^{18}O_{TRC}$, with only a few variables showing significant effects in isolated months.

Overall, correlation analyses between $\delta^{18}O_{TRC}$ and local climate factors indicate that all three sites consistently capture hydroclimatic variability. Results based on first-differenced chronologies further support these patterns (Fig. S3). Correlation strengths at the northern site changed little after differencing, whereas correlations with moisture-related indices become stronger at the central and southern sites, indicating that the interannual correspondence between $\delta^{18}O_{TRC}$ and hydroclimate becomes clearer once low-frequency variability is reduced (Fig. S3). Notably, at the northern site, the original four-tree and expanded seven-tree chronologies also showed broadly consistent climate-response patterns, particularly for summer hydroclimatic variables (Fig. S2b, c).

In addition to the moisture signal, $\delta^{18}O_{TRC}$ at all three sites also exhibits significant temperature responses. The central site shows the strongest summer temperature signal, with $\delta^{18}O_{TRC}$ correlated with June–September T_{max} ($r = 0.45$, $p < 0.01$, $n = 71$) (Fig. 3), and this relationship remains nearly unchanged when using first-differenced series (Fig. S3). Notably, the temperature influence is not confined to summer, but extends into the previous cold season and the current spring. Further analyses show stronger correlations between $\delta^{18}O_{TRC}$ and broader seasonal temperature windows: the northern site correlates with March–September T_{max} ($r = 0.50$), while the central and southern sites correlate with mean temperature from the previous October to the current September (both $r = 0.48$), exceeding the strength of summer-only temperature signals.



297

298 Figure 3. Correlations between $\delta^{18}O_{TRC}$ and meteorological factors for the northern (a), central (b), and southern (c)
299 sites in the East European Plain. The time periods are 1950–2021 (north), 1950–2020 (central), and 1950–2014
300 (south), except for SPEI (1950–2018) at the northern and central sites and SM (1982 to the end year of each
301 chronology) at all sites. T_{mean} and precipitation were obtained from meteorological stations, except that precipitation
302 at the central site was taken from the CRU TS 4.08 dataset.

303 Source-water signals in the three $\delta^{18}O_{TRC}$ chronologies are shown in Fig. 4. At all sites, $\delta^{18}O_{TRC}$
304 showed its strongest correlations with $\delta^{18}O_p$ in early summer (June–July), with r = 0.47, 0.68, and 0.42
305 from north to south ($p < 0.01$; Fig. 4). Following first-order differencing, these correlations changed only
306 slightly (Fig. S4). At the northern site, $\delta^{18}O_{TRC}$ was also positively correlated with $\delta^{18}O_p$ in January and
307 March of the current year. At the central site, $\delta^{18}O_p$ in the previous September, October, and December,
308 as well as in January and May of the current year, was positively associated with $\delta^{18}O_{TRC}$. In contrast, at
309 the southern site, $\delta^{18}O_p$ outside June–July showed no significant relationship with $\delta^{18}O_{TRC}$.

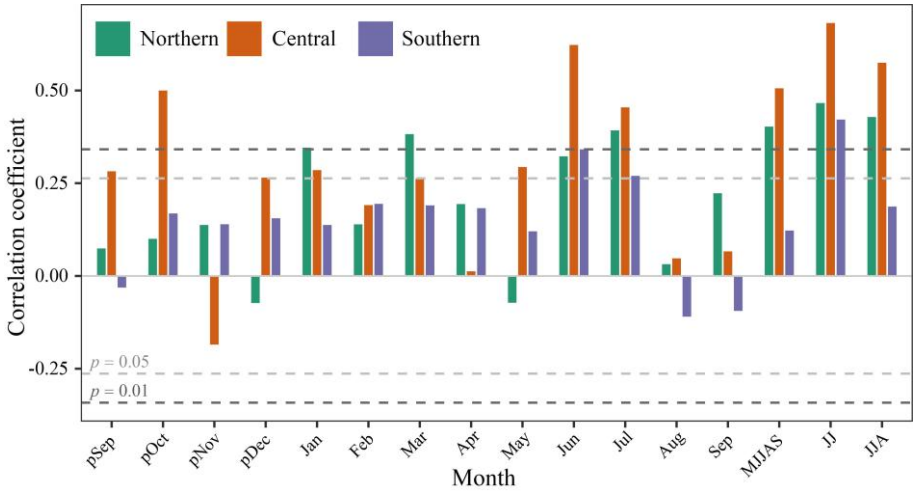


Figure 4. Correlations between $\delta^{18}O_{TRC}$ and $\delta^{18}O_p$ (1958–2013).

For the spatial difference between the northern and central sites (NC), the $\delta^{18}O_{TRC}$ difference is −1.288‰. In this case, $\Delta\delta^{18}O_p$ (−1.159‰) is larger than the difference in the enrichment term (−0.688‰), indicating that source-water isotopic differences dominate the NC $\delta^{18}O_{TRC}$ spatial offset (Table 2). In contrast, the $\delta^{18}O_{TRC}$ difference between the central and southern sites (CS) is −2.884‰, and the enrichment-term difference (−2.242‰) exceeds $\Delta\delta^{18}O_p$ (−1.295‰). Together with the larger RH difference (ΔRH = 10.174%), this suggests that stronger evaporative enrichment is the primary driver of the $\delta^{18}O_{TRC}$ offset between the Central and Southern sites (Table 2). The overall difference between the $\delta^{18}O_{TRC}$ from northern and southern sites (NS) is −4.172‰, with comparable magnitudes for $\Delta\delta^{18}O_p$ (−2.454‰) and the enrichment term (−2.930‰) (Table 2). Estimates based on observed $\delta^{18}O_p$ also support this pattern, showing a consistent north–south gradient (Table S7).

Table 2. Pairwise differences (Δ) in $\delta^{18}O_{TRC}$, modeled $\delta^{18}O_p$, RH, and the RH-driven enrichment term (May–September mean, 1958–2013; NC = North−Central, CS = Central−Southern, NS = North−Southern).

Pair	$\Delta\delta^{18}O_{TRC}$	$\Delta\delta^{18}O_p$	ΔRH	Δ*E*
NC	–1.288	–1.159	3.121	–0.688
CS	–2.884	–1.295	10.174	–2.242
NS	–4.172	–2.454	13.295	–2.930

3.3 Spatial correlations of $\delta^{18}O_{TRC}$ with hydroclimate and $\delta^{18}O_p$

Spatial correlation analyses based on gridded hydroclimate metrics (SPEI, VPD, and RH) indicate that $\delta^{18}O_{TRC}$ at all three sites exhibited a consistent response to regional summer moisture conditions: it

shows significant positive correlations with June–August VPD over broad areas, but significant negative correlations with RH and SPEI (Fig. 5). At the northern site, the strongest correlations formed a spatially coherent significant region over the White Sea area and adjacent northern Europe (Fig. 5a, d, g). The central site showed a similar but weaker pattern, with significant regions mainly covering the central East European Plain and extending eastward (Fig. 5b, e, h). At the southern site, significant regions were primarily distributed over the southern East European Plain (Fig. 5c, f, i). In addition, spatial correlations with ECHAM5-wiso–simulated $\delta^{18}O_p$ further suggested a coherent source-water isotopic imprint in $\delta^{18}O_{TRC}$ (Fig. S5). Overall, $\delta^{18}O_{TRC}$ reflected both regional summer hydroclimate and $\delta^{18}O_p$ variability, with broadly consistent spatial patterns across sites but differing strengths.

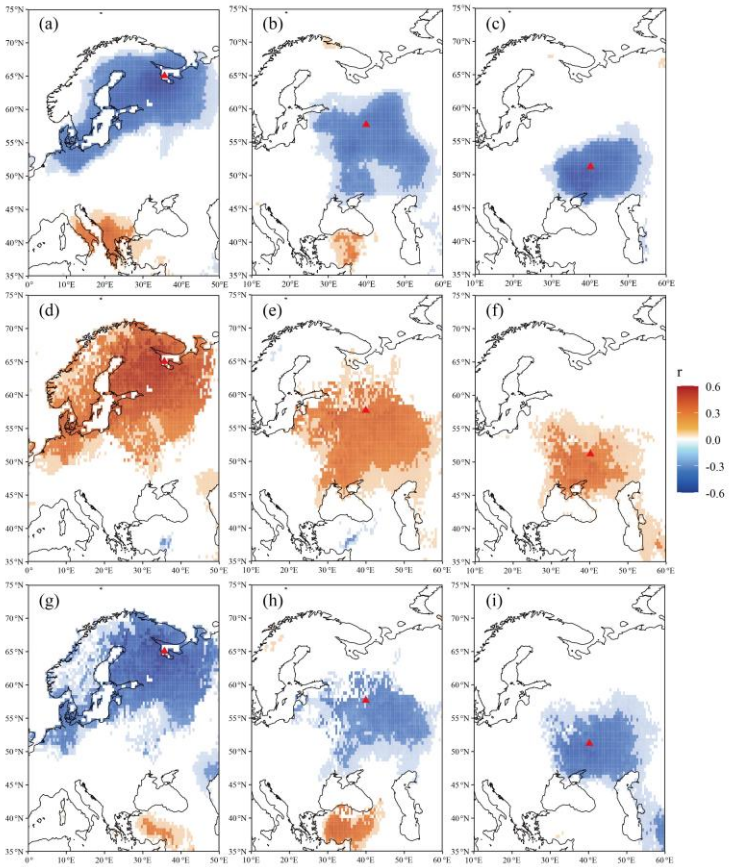


Figure 5. Spatial correlations between $\delta^{18}O_{TRC}$ and summer (June–August) hydroclimate variables: SPEI (a–c), VPD (d–f), and RH (g–i). Columns correspond to the northern (a, d, g), central (b, e, h), and southern (c, f, i) sites in the East European Plain; the corresponding year ranges are provided in the figure legend for Fig. 3.

3.4 Climate responses of tree-ring width

The climatic sensitivity of TRW differs markedly among the three sites (Fig. 6). Because the SM

record is relatively short, we do not use it as the primary basis for identifying dominant controls, although its correlations are significant. TRW at the northern and southern sites shows significant summer hydroclimate sensitivity, with the strongest relationships in both cases occurring for PDSI (north: July, r = 0.36; south: June–September, r = 0.54; Fig. 6a, c). By contrast, TRW at the central site shows little evidence of a stable moisture response (Fig. 6b). TRW at all three sites is also significantly sensitive to temperature, but the optimal response window shifts earlier toward lower latitudes: the northern site responds mainly to midsummer (July–August) temperature, the central site to early spring (March–April), and the southern site to late winter–early spring (January–March) (Fig. 6). Overall, the climatic responses of TRW exhibit clear regional differentiation: temperature and moisture signals are of comparable strength at the northern site, the central site is dominated by temperature, and the southern site is primarily controlled by moisture conditions.

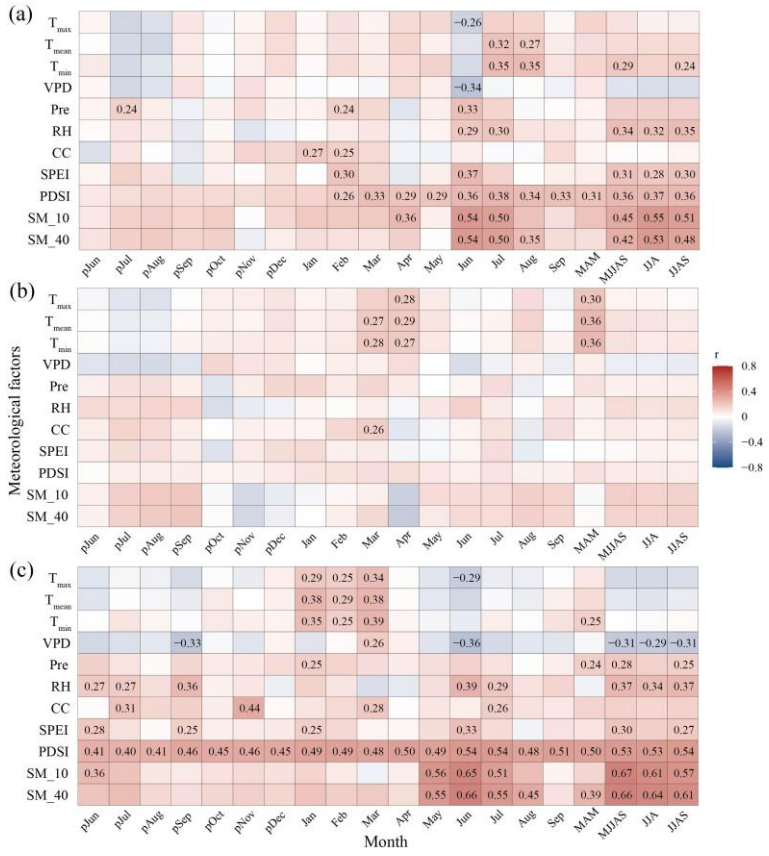


Figure 6. Correlations between TRW and meteorological factors for the northern (a), central (b), and southern (c) sites in the East European Plain. Time periods and meteorological data sources are the same as in Fig. 3, except that the northern TRW chronology spans 1950–2016. Numbers shown in the figure indicate correlations significant at $p < 0.05$.

4 Discussion

4.1 Spatial latitudinal gradient of $\delta^{18}O_{TRC}$ across the East European Plain

$\delta^{18}O_p$ and RH-regulated leaf-water evaporative enrichment jointly control spatial variations in $\delta^{18}O_{TRC}$ (Roden et al., 2000). Across the East European Plain, $\delta^{18}O_p$ shows higher values in the south than in the northern region (Fig. S6), whereas regional RH exhibits a wetter north–drier south gradient (Fig. 1). These large-scale gradients are broadly consistent with the southward increase in $\delta^{18}O_{TRC}$ across the region (Table 1; Fig. 2). Further analyses indicate that the dominant controlling factors on the spatial variability of $\delta^{18}O_{TRC}$ are different between the NC and CS site pairs.

For the NC pair, the between-site difference in $\delta^{18}O_p$ is clearly larger than the corresponding difference in RH-driven evaporative enrichment (Table 2), indicating that $\delta^{18}O_p$ is the primary driver. This pattern is expected because $\delta^{18}O_{TRC}$ partly reflects the isotopic composition of source water via soil-water uptake and therefore often covaries positively with $\delta^{18}O_p$ (Saurer et al., 2000). In mid- to high-latitude regions, the "amount effect" is generally weak, whereas temperature often exerts a dominant control on $\delta^{18}O_p$ (Krklec et al., 2018; Rozanski et al., 1992). At higher latitudes, lower condensation temperatures and stronger isotopic fractionation, together with progressive rainout during poleward transport, deplete ^{18}O in the remaining vapor and result in lower $\delta^{18}O_p$ values (Dansgaard, 1953; Gat, 1996). Global observations support this mechanism, showing an average decrease of ~0.5‰ per 1° increase in latitude (Rozanski et al., 1992). In addition, the RH difference between the northern and central sites is relatively small (Fig. 1; Fig. S6), resulting in a relatively limited between-site contrast in evaporative enrichment. Together, these mechanisms explain why source-water isotopes dominate spatial difference in $\delta^{18}O_{TRC}$ between the NC sites.

For the CS pair, the RH contrast is much larger than that in the NC pair (Fig. 1; Fig. S6). Consistently, the between-site difference in RH-driven evaporative enrichment exceeds the corresponding difference in $\delta^{18}O_p$ (Table 2), indicating that drier southern conditions enhance evaporative enrichment and contribute more to $\Delta\delta^{18}O_{TRC}$. Lower RH strengthens the leaf-to-atmosphere evaporative gradient, increasing ^{18}O enrichment in leaf water and its transfer to cellulose (Roden et al., 2000). A modeling study further indicates that spatial variation in leaf-water evaporative enrichment is closely linked to atmospheric humidity, with drier conditions favoring greater ^{18}O enrichment (Keel et al., 2016). Similar humidity-driven patterns have been reported elsewhere, for example along a north–south gradient in the

tropical Andes, where $\delta^{18}O_{TRC}$ increases toward drier southern sites (Álvarez et al., 2024).

Comparable large-scale latitudinal patterns in $\delta^{18}O_{TRC}$ has also been documented in other regions, including the European tree-ring $\delta^{18}O$ network (Balting et al., 2021), the Asian tree-ring $\delta^{18}O$ network (Huang et al., 2025; Xu et al., 2021, 2024), and eastern Anatolia (Mutlu et al., 2012). Across Europe, spatial variability in tree-ring $\delta^{18}O$ has been attributed to the combined effects of latitude, elevation, and continentality (Balting et al., 2021; Mutlu et al., 2012). Across Asia, the tripolar pattern in tree-ring $\delta^{18}O$ primarily reflects the latitudinal structure of $\delta^{18}O_p$, with RH-controlled enrichment acting as a key modulator, particularly in mid-latitudes (Huang et al., 2025; Xu et al., 2024). Similar to patterns reported in Asian, spatial variability in the East European Plain reflects a dual control: the mid- to high-latitude NC pair is dominated by $\delta^{18}O_p$, whereas the mid-latitude CS pair is driven primarily by RH-controlled enrichment. Together, these mechanisms produce a south-to-north decrease in $\delta^{18}O_{TRC}$ across the region.

4.2 Interannual climatic implications of $\delta^{18}O_{TRC}$ in the East European Plain

Based on the mechanistic framework of cellulose $\delta^{18}O$, $\delta^{18}O_{TRC}$ integrates both $\delta^{18}O_p$ and evaporative enrichment of leaf water (McCarroll and Loader, 2004; Roden et al., 2000). Across the three sites, $\delta^{18}O_{TRC}$ records a coherent interannual signal during the growing season and summer: values tend to increase under higher evaporative demand and more enriched $\delta^{18}O_p$, and decrease under more humid conditions (Fig. 3; Fig. S3).

On the source-water side, interannual variability in source-water $\delta^{18}O$ is linked to temperature- and precipitation-related processes (Dansgaard, 1964; Rozanski et al., 1992). Higher temperature and VPD can enhance soil evaporation and enrich near-surface soil water, whereas higher precipitation and SM tend to reduce evaporative enrichment and $\delta^{18}O_s$. In parallel, the strong linkages of $\delta^{18}O_{TRC}$ with moisture indicate leaf-water evaporative enrichment as a key control (McCarroll and Loader, 2004; Roden et al., 2000), because root uptake involves negligible isotopic fractionation (Dawson and Ehleringer, 1991). Lower RH (higher VPD) enhances leaf-water ^{18}O enrichment and its transfer to cellulose (McCarroll and Loader, 2004; Roden et al., 2000); CC likely reflects coupled radiative–humidity effects on enrichment (Wang et al., 2022). Finally, SPEI and PDSI integrate precipitation supply and evaporative demand (Dai et al., 2004; Vicente-Serrano et al., 2010b), which is consistent with their coherent relationships with $\delta^{18}O_{TRC}$ as integrated indicators of hydroclimate (Xu et al., 2013a).

Despite the overall similarity in response patterns, the dominant controls on interannual $\delta^{18}O_{TRC}$

variability differ among sites. The central site exhibits both a pronounced source-water isotopic imprint and a leaf-water enrichment signal (Fig. 3–4; Fig. S3). Significant correlations between $\delta^{18}O_{TRC}$ and $\delta^{18}O_p$ in both the original and first-differenced series indicate that interannual anomalies in source-water $\delta^{18}O$ are effectively transmitted into cellulose. Together with the relatively larger interannual variability in $\delta^{18}O_p$ and smaller variability in RH (Fig. S6), this suggests that the source-water signal is more readily expressed statistically. By contrast, correlations with humidity-related metrics become markedly stronger after differencing, indicating that low-frequency variability partly obscures the interannual hydroclimate signal (Fig. S3). The weaker humidity signal in the original series may reflect the urban forest-park setting of the central site, where canopy buffering and local anthropogenic influences can decouple near-canopy humidity from the broader gridded macroclimatic background at low frequencies (De Frenne et al., 2019; Zellweger et al., 2020). In addition, the strong T_{max} response changes little after differencing, implying that it is not solely trend-driven and may partly reflect temperature-related modulation of regional $\delta^{18}O_p$ and associated processes (Field et al., 2022; Leland et al., 2023).

In contrast, humidity signals are more pronounced at the northern and southern sites, although the underlying mechanisms differ. The northern $\delta^{18}O_{TRC}$ chronology shows a stable VPD signal (Fig. 3; Fig. S3; Fig. S7). The Solovetsky Islands lie in a cold and moist high-latitude environment (Fig. 1), where tree growth is more strongly temperature-limited. Under such conditions, warming tends to increase atmospheric evaporative demand (Zharkov et al., 2021), allowing evaporative-demand–driven leaf-water enrichment to exert a stable control on interannual $\delta^{18}O_{TRC}$ variability. Similarly, studies from high-latitude northern Europe have reported clear summer VPD signals in $\delta^{18}O_{TRC}$ and have used $\delta^{18}O_{TRC}$ networks to reconstruct regional-scale VPD (Treydte et al., 2024). By comparison, the southern site is characterized by a drier climatic background with lower RH (Fig. 1; Fig. S6), and $\delta^{18}O_{TRC}$ shows its strongest relationship with SPEI, consistent with evaporative enrichment being jointly constrained by moisture supply and atmospheric demand. Numerous SPEI reconstructions based on $\delta^{18}O_{TRC}$ have also been reported for mid-latitude Europe (An et al., 2023; Freund et al., 2023; Labuhn et al., 2016).

Together, these results highlight the potential of $\delta^{18}O_{TRC}$ for hydroclimate reconstructions in the East European Plain. The northern $\delta^{18}O_{TRC}$ chronology exhibits a strong and stable growing-season VPD signal (Fig. 3; Fig. S3; Fig. S7), indicating particularly strong potential for high-latitude hydroclimate reconstruction. Meanwhile, the significant coherence among chronologies from nearby sites (Fig. 2e), together with the common sensitivity of the three chronologies to regional summer hydroclimate (Fig.

5), underscores the potential of $\delta^{18}O_{TRC}$ for reconstructing regional-scale hydroclimate variability and supports expanding site coverage to improve the spatial representativeness of future reconstructions. However, the low replication and EPS values of 0.84 at the central and southern sites introduce uncertainty in chronology representativeness and should be considered when evaluating their regional applicability and reconstruction potential.

4.3 Compared with TRW, $\delta^{18}O_{TRC}$ provide additional information

Moisture signals in TRW at the northern and central sites are markedly weaker than those in $\delta^{18}O_{TRC}$ (Fig. 3; Fig. 6). This contrast is consistent with the growth limitation commonly observed at mid- to high latitudes, where TRW north of approximately 50–60° N is often primarily constrained by summer temperature and is therefore better suited for temperature reconstructions (Dolgova et al., 2022; Solomina and Matskovsky, 2021). By contrast, $\delta^{18}O_{TRC}$ reflects both source-water isotope composition and leaf-water evaporative enrichment, allowing it to retain sensitivity to atmospheric humidity and evaporative demand even when radial growth is not strongly moisture-limited (McCarroll and Loader, 2004; Roden et al., 2000). Thus, in relatively humid, temperature-limited mid- to high-latitude settings, $\delta^{18}O_{TRC}$ may outperform TRW in characterizing hydroclimate variability.

At the drier southern site, the strongest correlation between TRW and PDSI is comparable in magnitude to the strongest correlation between $\delta^{18}O_{TRC}$ and SPEI (Fig. 3; Fig. 6). In addition, relative to other humidity metrics, $\delta^{18}O_{TRC}$ shows weaker associations with PDSI in both the original and first-differenced series, whereas TRW mainly reflects PDSI and SM signals (Fig. 6). Because PDSI is widely used to represent drought severity and persistence and is closely related to soil-moisture conditions (Dai et al., 2004), this suggests that under stronger moisture limitation, TRW more directly tracks soil-moisture constraints on radial growth. By contrast, SPEI integrates precipitation supply and potential evapotranspiration and therefore better represents moisture conditions shaped jointly by water supply and atmospheric demand (Vicente-Serrano et al., 2010a). Accordingly, at the drier southern site, TRW tends to preferentially capture soil-moisture variability, whereas $\delta^{18}O_{TRC}$ is more likely to integrate both source-water signals and evaporative enrichment processes.

The contrasting climate responses of $\delta^{18}O_{TRC}$ and TRW observed in this study indicate that different tree-ring proxies record complementary climatic information. Previous studies have shown that, in temperature-limited environments, maximum latewood density (MXD) and some quantitative wood-

anatomical traits generally exhibit stronger warm-season temperature signals than TRW and have been widely used to reconstruct warm-season temperature variability (Björklund et al., 2019, 2023). By contrast, stable carbon and oxygen isotopes can provide complementary information on tree physiological responses and hydroclimatic processes (McCarroll and Loader, 2004). Therefore, future multiproxy studies combining TRW, MXD, quantitative wood anatomy, and stable carbon and oxygen isotopes across the East European Plain could help more effectively disentangle regional temperature and moisture signals.

5 Conclusions

We established three $\delta^{18}O_{TRC}$ chronologies of Scots pine over the East European Plain. We found a clear latitudinal gradient, with lower $\delta^{18}O_{TRC}$ values in the north and higher values in the south. Across sites, $\delta^{18}O_{TRC}$ shows broadly similar response patterns to growing-season and summer climate variables, as well as to $\delta^{18}O_p$, although the dominant controls and response strengths differ among sites. The $\delta^{18}O_{TRC}$ chronologies at three sites record a coherent signal of regional summer hydroclimate variability, but the northern chronology shows the strongest and most stable climate response, indicating the greatest reconstruction potential. In addition, comparison with TRW suggests that $\delta^{18}O_{TRC}$ may be the more suitable hydroclimate proxy in temperature-limited environments, whereas in drier, moisture-limited settings TRW more directly reflects soil-moisture constraints on radial growth, while $\delta^{18}O_{TRC}$ more likely integrates source-water isotopic signals and evaporative enrichment processes. Overall, our study demonstrates that $\delta^{18}O_{TRC}$ contains valuable information on the spatiotemporal patterns of hydroclimate variability across the East European Plain and highlights its potential for future hydroclimate reconstruction.

Data availability. The raw data supporting the conclusions of this article will be made available by the corresponding author Chenxi Xu, (cxxu@mail.iggcas.ac.cn).

Author contributions. CX, WA, and VM conceived the study. QL performed the data analysis and prepared the original draft with contributions from CX, WA, and RH. CX and TZ acquired funding for this study. OS, VM, and ED collected the samples and provided the tree-ring width data. All authors

contributed to the interpretation of the results, critically reviewed and edited the final manuscript, and approved the submitted version.

Competing interests. The contact author has declared that none of the authors has any competing interests.

Acknowledgments. We are grateful to Qingyu Zhao, Sainan Liu, and Yao Li for providing relevant references and helpful suggestions during figure preparation and manuscript preparation.

Financial support. This study is supported by the International Partnership program of the Chinese Academy of Sciences (Grant Number: 170GJHZ2023074GC), National Key Research and Development Program of China (Grant Number: 2024YFF0807902), the Second Tibetan Plateau Scientific Expedition and Research (STEP) program (2024QZKK0301).

References

Allen, R. G., Pereira, L. S., Raes, D., and Smith, M.: Crop evapotranspiration – Guidelines for computing crop water requirements, FAO Irrigation and Drainage Paper 56, FAO, Rome, 1998.

Allison, G. B., Gat, J. R., and Leaney, F. W. J.: The relationship between deuterium and oxygen-18 delta values in leaf water, Chem. Geol. Isot. Geosci. Sect., 58, 145–156, https://doi.org/10.1016/0168-9622(85)90035-1, 1985.

Álvarez, C., Christie, D. A., González-Reyes, Á., Veblen, T. T., Helle, G., LeQuesne, C., Rodriguez-Caton, M., Szejner, P., Flores-Sáez, F., Gipoulou-Zúñiga, T., Suazo-Álvarez, M., Muñoz-Salazar, T., Aliste, D., Morales, M. S., Muñoz, A., and Villalba, R.: Hydroclimate variability in the Tropical Andes recorded by $\delta^{18}O$ isotopes from a new network of *Polylepis tarapacana* tree-rings, Glob. Planet. Change, 239, 104503, https://doi.org/10.1016/j.gloplacha.2024.104503, 2024.

An, W., Xu, C., Marković, S. B., Sun, S., Sun, Y., Gavrilov, M. B., Govedar, Z., Hao, Q., and Guo, Z.: Anthropogenic warming has exacerbated droughts in southern Europe since the 1850s, Commun. Earth Environ., 4, 232, https://doi.org/10.1038/s43247-023-00907-1, 2023.

Arosio, T., Leuenberger, M., Nicolussi, K., Esper, J., Krusic, P. J., Bebchuk, T., Tegel, W., Hafner, A., Kirdyanov, A., Schlüchter, C., Reinig, F., Muschitiello, F., and Büntgen, U.: Tree-ring stable isotopes from the European Alps reveal long-term summer drying over the Holocene, Sci. Adv., 11, eadr4161, https://doi.org/10.1126/sciadv.adr4161, 2025.

Balting, D. F., Ionita, M., Wegmann, M., Helle, G., Schleser, G. H., Rimbu, N., Freund, M. B., Heinrich, I., Caldarescu, D., and Lohmann, G.: Large-scale climate signals of a European oxygen isotope network from tree rings, Clim. Past, 17, 1005–1023, https://doi.org/10.5194/cp-17-1005-2021, 2021.

Barbour, M. M.: Stable oxygen isotope composition of plant tissue: a review, Funct. Plant Biol., 34, 83–94, https://doi.org/10.1071/FP06228, 2007.

Björklund, J., von Arx, G., Nievergelt, D., Wilson, R., Van den Bulcke, J., Günther, B., Loader, N. J., Rydval, M., Fonti, P., Scharnweber, T., Andreu-Hayles, L., Büntgen, U., D'Arrigo, R., Davi, N., De Mil, T., Esper, J., Gärtner, H., Geary, J., Gunnarson, B. E., Hartl, C., Hevia, A., Song, H., Janecka, K., Kaczka, R. J., Kirdyanov, A. V., Kochbeck, M., Liu, Y., Meko, M., Mundo, I., Nicolussi, K., Oelkers, R., Pichler, T., Sánchez-Salguero, R., Schneider, L., Schweingruber, F., Timonen, M., Trouet, V., Van Acker, J., Verstege, A., Villalba, R., Wilmking, M., and Frank, D.: Scientific Merits and Analytical Challenges of Tree-Ring Densitometry, Rev. Geophys., 57, 1224–1264, https://doi.org/10.1029/2019RG000642, 2019.

Björklund, J., Seftigen, K., Stoffel, M., Fonti, M. V., Kottlow, S., Frank, D. C., Esper, J., Fonti, P., Goosse, H., Grudd, H., Gunnarson, B. E., Nievergelt, D., Pellizzari, E., Carrer, M., and von Arx, G.: Fennoscandian tree-ring anatomy shows a warmer modern than medieval climate, Nature, 620, 97–103, https://doi.org/10.1038/s41586-023-06176-4, 2023.

Cook, E. R., Solomina, O., Matskovsky, V., Cook, B. I., Agafonov, L., Berdnikova, A., Dolgova, E., Karpukhin, A., Knysh, N., Kulakova, M., Kuznetsova, V., Kyncl, T., Kyncl, J., Maximova, O., Panyushkina, I., Seim, A., Tishin, D., Ważny, T., and Yermokhin, M.: The European Russia Drought Atlas (1400–2016 CE), Clim. Dyn., 54, 2317–2335, https://doi.org/10.1007/s00382-019-05115-2, 2020.

Dai, A., Trenberth, K. E., and Qian, T.: A Global Dataset of Palmer Drought Severity Index for 1870–2002: Relationship with Soil Moisture and Effects of Surface Warming, J. Hydrometeorol., 5, 1117–1130, https://doi.org/10.1175/JHM-386.1, 2004.

Dansgaard, W.: The Abundance of O^{18} in Atmospheric Water and Water Vapour, Tellus, 5, 461–469, https://doi.org/10.1111/j.2153-3490.1953.tb01076.x, 1953.

Dansgaard, W.: Stable isotopes in precipitation, Tellus, 16, 436–468, https://doi.org/10.1111/j.2153-3490.1964.tb00181.x, 1964.

Dawson, T. E. and Ehleringer, J. R.: Streamside trees that do not use stream water, Nature, 350, 335–337, https://doi.org/10.1038/350335a0, 1991.

De Frenne, P., Zellweger, F., Rodríguez-Sánchez, F., Scheffers, B. R., Hylander, K., Luoto, M., Vellend, M., Verheyen, K., and Lenoir, J.: Global buffering of temperatures under forest canopies, Nat. Ecol. Evol., 3, 744–749, https://doi.org/10.1038/s41559-019-0842-1, 2019.

Dolgova, E. A., Solomina, O. N., Matskovsky, V. V., Cherenkova, E. A., and Semenyak, N. S.: Climate signal strength in tree-ring width of spruce growing in the Solovetsky Islands (Russia), Dendrochronologia, 76, 126012, https://doi.org/10.1016/j.dendro.2022.126012, 2022.

Field, R. D., Andreu-Hayles, L., D'Arrigo, R. D., Oelkers, R., Luckman, B. H., Morimoto, D., Boucher,

572 E., Gennaretti, F., Hermoso, I., Lavergne, A., and Levesque, M.: Tree-ring cellulose $\delta^{18}O$ records similar
573 large-scale climate influences as precipitation $\delta^{18}O$ in the Northwest Territories of Canada, Clim. Dyn.,
574 58, 759–776, https://doi.org/10.1007/s00382-021-05932-4, 2022.

575 Freund, M. B., Helle, G., Balting, D. F., Ballis, N., Schleser, G. H., and Cubasch, U.: European tree-ring
576 isotopes indicate unusual recent hydroclimate, Commun. Earth Environ., 4, 26,
577 https://doi.org/10.1038/s43247-022-00648-7, 2023.

578 Gat, J. R.: Oxygen and hydrogen isotopes in the hydrologic cycle, Annu. Rev. Earth Planet. Sci., 24,
579 225–262, https://doi.org/10.1146/annurev.earth.24.1.225, 1996.

580 Harris, I., Osborn, T. J., Jones, P., and Lister, D.: Version 4 of the CRU TS monthly high-resolution
581 gridded multivariate climate dataset, Sci. Data, 7, 109, https://doi.org/10.1038/s41597-020-0453-3, 2020.

582 Haupt, M., Weigl, M., Grabner, M., and Boettger, T.: A 400-year reconstruction of July relative air
583 humidity for the Vienna region (eastern Austria) based on carbon and oxygen stable isotope ratios in
584 tree-ring latewood cellulose of oaks (*Quercus petraea* Matt. Liebl.), Clim. Change, 105, 243–262,
585 https://doi.org/10.1007/s10584-010-9862-1, 2011.

586 Holmes, R. L.: Computer-assisted quality control in tree-ring dating and measurement, Tree-Ring Bull.,
587 43, 69–78, 1983.

588 Huang, R., Xu, C., An, W., Zhao, Q., Zhao, Y., Liu, Y., Grießinger, J., Meier, W. J.-H., and Guo, Z.:
589 Asian continental isoscapes of tree-ring $\delta^{18}O$: implications for paleoclimate and paleoenvironment, Natl.
590 Sci. Rev., 12, nwaf481, https://doi.org/10.1093/nsr/nwaf481, 2025.

591 Hughes, M. K., Olchev, A., Bunn, A. G., Berner, L. T., Losleben, M., and Novenko, E.: Different climate
592 responses of spruce and pine growth in Northern European Russia, Dendrochronologia, 56, 125601,
593 https://doi.org/10.1016/j.dendro.2019.05.005, 2019.

594 Keel, S. G., Joos, F., Spahni, R., Saurer, M., Weigt, R. B., and Klesse, S.: Simulating oxygen isotope
595 ratios in tree ring cellulose using a dynamic global vegetation model, Biogeosciences, 13, 3869–3886,
596 https://doi.org/10.5194/bg-13-3869-2016, 2016.

597 Klimenko, V. and Solomina, O.: Climatic Variations in the East European Plain During the Last
598 Millennium: State of the Art, in: The Polish Climate in the European Context: An Historical Overview,
599 edited by: Przybylak, R., Springer Netherlands, Dordrecht, 71–101, https://doi.org/10.1007/978-90-481-
600 3167-9_3, 2010.

601 Krklec, K., Domínguez-Villar, D., and Lojen, S.: The impact of moisture sources on the oxygen isotope
602 composition of precipitation at a continental site in central Europe, J. Hydrol., 561, 810–821,
603 https://doi.org/10.1016/j.jhydrol.2018.04.045, 2018.

604 Kuznetsova, V. V. and Solomina, O. N.: Contrasting climate signals across a Scots pine (*Pinus sylvestris*
605 L.) tree-ring network in the Middle Volga (European Russia), Dendrochronologia, 73, 125957,
606 https://doi.org/10.1016/j.dendro.2022.125957, 2022.

Labuhn, I., Daux, V., Girardclos, O., Stievenard, M., Pierre, M., and Masson-Delmotte, V.: French summer droughts since 1326 CE: a reconstruction based on tree ring cellulose $\delta^{18}O$, Clim. Past, 12, 1101–1117, https://doi.org/10.5194/cp-12-1101-2016, 2016.

Lange, J., Buras, A., Cruz-García, R., Gurskaya, M., Jalkanen, R., Kukarskih, V., Seo, J.-W., and Wilmking, M.: Climate Regimes Override Micro-Site Effects on the Summer Temperature Signal of Scots Pine at Its Northern Distribution Limits, Front. Plant Sci., 9, 1597, https://doi.org/10.3389/fpls.2018.01597, 2018.

Langebroek, P. M., Werner, M., and Lohmann, G.: Climate information imprinted in oxygen-isotopic composition of precipitation in Europe, Earth Planet. Sci. Lett., 311, 144–154, https://doi.org/10.1016/j.epsl.2011.08.049, 2011.

Leland, C., Andreu-Hayles, L., Cook, E. R., Anchukaitis, K. J., Byambasuren, O., Davi, N., Hessl, A., Martin-Benito, D., Nachin, B., and Pederson, N.: Impacts of climate and tree morphology on tree-ring stable isotopes in central Mongolia, Tree Physiol., 43, 539–555, https://doi.org/10.1093/treephys/tpac142, 2023.

Liu, Y., Wang, L., Zhou, W., and Chen, W.: Three Eurasian teleconnection patterns: spatial structures, temporal variability, and associated winter climate anomalies, Clim. Dyn., 42, 2817–2839, https://doi.org/10.1007/s00382-014-2163-z, 2014.

Loader, N. J., Robertson, I., Barker, A. C., Switsur, V. R., and Waterhouse, J. S.: An improved technique for the batch processing of small wholewood samples to α-cellulose, Chem. Geol., 136, 313–317, https://doi.org/10.1016/S0009-2541(96)00133-7, 1997.

Matskovsky, V.: Climatic signal in tree-ring width chronologies of conifers in European Russia, Int. J. Climatol., 36, 3398–3406, https://doi.org/10.1002/joc.4563, 2016.

Matskovsky, V., Dolgova, E., Lomakin, N., and Matveev, S.: Dendroclimatology and historical climatology of Voronezh region, European Russia, since 1790s, Int. J. Climatol., 37, 3057–3066, https://doi.org/10.1002/joc.4896, 2017.

Matskovsky, V. V., Kuznetsova, V. V., Semenyak, N. S., Turchinskaya, S. M., Zazovskaya, E. P., Engovatova, A. V., Lazarev, A. S., Zhdanova, E. Yu., Dolgova, E. A., and Solomina, O. N.: Dendroclimatic potential of stable carbon isotopes in tree-ring cellulose of *Pinus sylvestris* L. in the Yaroslavl and Kostroma regions [in Russian], Geomorfologiya i Paleogeografiya, 53, 74–82, https://doi.org/10.31857/S0435428122030099, 2022.

Matulewski, P., Buchwal, A., and Makohonienko, M.: Higher climatic sensitivity of Scots pine (*Pinus sylvestris* L.) subjected to tourist pressure on a hiking trail in the Brodnica Lakeland, NE Poland, Dendrochronologia, 54, 78–86, https://doi.org/10.1016/j.dendro.2019.02.008, 2019.

Matveev, S., Timashchuk, D., and Matskovsky, V.: The intensity of the climatic signal in the dynamics of the increment of Scots pine (Pinus silvestris L.) of the Khrenovskii forest (Voronezh region, Russia), IOP Conf. Ser. Earth Environ. Sci., 226, 012017, https://doi.org/10.1088/1755-1315/226/1/012017, 2019.

Matveev, S., Tishin, D., Maximchuk, P., and Zhuravleva, I.: Seasonal radial growth dynamics of Scots pine (*Pinus silvestris* L.) in Voronezh region (Russia), IOP Conf. Ser. Earth Environ. Sci., 595, 012044, https://doi.org/10.1088/1755-1315/595/1/012044, 2020.

Matveev, S. M., Chendev, Yu. G., Lupo, A. R., Hubbart, J. A., and Timashchuk, D. A.: Climatic Changes in the East-European Forest-Steppe and Effects on Scots Pine Productivity, Pure Appl. Geophys., 174, 427–443, https://doi.org/10.1007/s00024-016-1420-y, 2017.

McCarroll, D. and Loader, N. J.: Stable isotopes in tree rings, Quat. Sci. Rev., 23, 771–801, https://doi.org/10.1016/j.quascirev.2003.06.017, 2004.

McNally, A., Arsenault, K., Kumar, S., Shukla, S., Peterson, P., Wang, S., Funk, C., Peters-Lidard, C. D., and Verdin, J. P.: A land data assimilation system for sub-Saharan Africa food and water security applications, Sci. Data, 4, 170012, https://doi.org/10.1038/sdata.2017.12, 2017.

Moberg, A., Jones, P. D., Lister, D., Walther, A., Brunet, M., Jacobeit, J., Alexander, L. V., Della-Marta, P. M., Luterbacher, J., Yiou, P., Chen, D., Klein Tank, A. M. G., Saladié, O., Sigró, J., Aguilar, E., Alexandersson, H., Almarza, C., Auer, I., Barriendos, M., Begert, M., Bergström, H., Böhm, R., Butler, C. J., Caesar, J., Drebs, A., Founda, D., Gerstengarbe, F., Micela, G., Maugeri, M., Österle, H., Pandzic, K., Petrakis, M., Srnec, L., Tolasz, R., Tuomenvirta, H., Werner, P. C., Linderholm, H., Philipp, A., Wanner, H., and Xoplaki, E.: Indices for daily temperature and precipitation extremes in Europe analyzed for the period 1901–2000, J. Geophys. Res.-Atmos., 111, D22106, https://doi.org/10.1029/2006JD007103, 2006.

Morozova, S. V., Denisov, K. E., Polyanskaya, E. A., Kondakov, K. S., Korotkova, N. V., and Gafurov, R. R.: Changes in the Atmospheric Circulation Regime in the Context of Global Climate Trends in the Atlantic-Eurasian Sector of the Northern Hemisphere, Geogr. Nat. Resour., 44, 191–197, https://doi.org/10.1134/S1875372823030083, 2023.

Mutlu, H., Köse, N., Akkemik, Ü., Aral, D., Kaya, A., Manning, S. W., Pearson, C. L., and Dalfes, N.: Environmental and climatic signals from stable isotopes in Anatolian tree rings, Turkey, Reg. Environ. Change, 12, 559–570, https://doi.org/10.1007/s10113-011-0273-2, 2012.

Nagavciuc, V., Michel, S. L. L., Balting, D. F., Helle, G., Freund, M., Schleser, G. H., Steger, D. N., Lohmann, G., and Ionita, M.: A past and present perspective on the European summer vapor pressure deficit, Clim. Past, 20, 573–595, https://doi.org/10.5194/cp-20-573-2024, 2024.

Panyushkina, I. P., Karpukhin, A. A., and Engovatova, A. V.: Moisture record of the Upper Volga catchment between AD 1430 and 1600 supported by a $\delta^{13}C$ tree-ring chronology of archaeological pine timbers, Dendrochronologia, 39, 24–31, https://doi.org/10.1016/j.dendro.2016.02.002, 2016.

Rinne, K.: 400-year May-August Precipitation Reconstruction for England Using Stable Oxygen Isotope Ratios ($\delta^{18}O$) of Tree Rings, Quat. Int., 279–280, 403–404, https://doi.org/10.1016/j.quaint.2012.08.1281, 2012.

Roden, J. S., Lin, G., and Ehleringer, J. R.: A mechanistic model for interpretation of hydrogen and oxygen isotope ratios in tree-ring cellulose, Geochim. Cosmochim. Acta, 64, 21–35,

https://doi.org/10.1016/S0016-7037(99)00195-7, 2000.

Römer, P., Wieland, A., Torbenson, M. C. A., Reinig, F., Ziaco, E., Frigo, D., Greule, M., Urban, O., Čáslavský, J., Pernicová, N., Trnka, M., Carrer, M., Büntgen, U., Keppler, F., and Esper, J.: Covariance and climate signals among state-of-the-art tree-ring proxies, Quat. Sci. Rev., 355, 109270, https://doi.org/10.1016/j.quascirev.2025.109270, 2025.

Rozanski, K., Araguás-Araguás, L., and Gonfiantini, R.: Relation Between Long-Term Trends of Oxygen-18 Isotope Composition of Precipitation and Climate, Science, 258, 981–985, https://doi.org/10.1126/science.258.5084.981, 1992.

Saurer, M., Cherubini, P., and Siegwolf, R.: Oxygen isotopes in tree rings of *Abies alba*: The climatic significance of interdecadal variations, J. Geophys. Res.-Atmos., 105, 12461–12470, https://doi.org/10.1029/2000JD900160, 2000.

Semenyak, N. and Dolgova, E.: Dendroclimatic signals in the pine and spruce chronologies in the Solovetsky Archipelago, Dendrochronologia, 77, 126029, https://doi.org/10.1016/j.dendro.2022.126029, 2023.

Solomina, O. and Matskovsky, V.: Dendrochronology in European Russia in the Early 21st Century: State of the Art, Front. Ecol. Evol., 9, 738199, https://doi.org/10.3389/fevo.2021.738199, 2021.

Spinoni, J., Naumann, G., Vogt, J., and Barbosa, P.: European drought climatologies and trends based on a multi-indicator approach, Glob. Planet. Change, 127, 50–57, https://doi.org/10.1016/j.gloplacha.2015.01.012, 2015.

Sternberg, L. and Ellsworth, P. F. V.: Divergent Biochemical Fractionation, Not Convergent Temperature, Explains Cellulose Oxygen Isotope Enrichment across Latitudes, PLoS ONE, 6, e28040, https://doi.org/10.1371/journal.pone.0028040, 2011.

Tishin, D. V., Chizhikova, N. A., Zhuravleva, I. V., and Chugunov, R. G.: Xylogenesis of Pinus sylvestris L. growing in the northern island ecosystems [in Russian], Lesotekhnicheskii Zhurnal (Forestry Engineering Journal), 6, 89–97, https://doi.org/10.12737/23439, 2016.

Treydte, K., Frank, D., Esper, J., Andreu, L., Bednarz, Z., Berninger, F., Boettger, T., D'Alessandro, C. M., Etien, N., Filot, M., Grabner, M., Guillemin, M. T., Gutierrez, E., Haupt, M., Helle, G., Hilasvuori, E., Jungner, H., Kalela-Brundin, M., Krapiec, M., Leuenberger, M., Loader, N. J., Masson-Delmotte, V., Pazdur, A., Pawelczyk, S., Pierre, M., Planells, O., Pukiene, R., Reynolds-Henne, C. E., Rinne, K. T., Saracino, A., Saurer, M., Sonninen, E., Stievenard, M., Switsur, V. R., Szczepanek, M., Szychowska-Krapiec, E., Todaro, L., Waterhouse, J. S., Weigl, M., and Schleser, G. H.: Signal strength and climate calibration of a European tree-ring isotope network, Geophys. Res. Lett., 34, L24302, https://doi.org/10.1029/2007GL031106, 2007.

Treydte, K., Boda, S., Graf Pannatier, E., Fonti, P., Frank, D., Ullrich, B., Saurer, M., Siegwolf, R., Battipaglia, G., Werner, W., and Gessler, A.: Seasonal transfer of oxygen isotopes from precipitation and soil to the tree ring: source water versus needle water enrichment, New Phytol., 202, 772–783, https://doi.org/10.1111/nph.12741, 2014.

Treydte, K., Liu, L., Padrón, R. S., Martínez-Sancho, E., Babst, F., Frank, D. C., Gessler, A., Kahmen, A., Poulter, B., Seneviratne, S. I., Stegehuis, A. I., Wilson, R., Andreu-Hayles, L., Bale, R., Bednarz, Z., Boettger, T., Berninger, F., Büntgen, U., Daux, V., Dorado-Liñán, I., Esper, J., Friedrich, M., Gagen, M., Grabner, M., Grudd, H., Gunnarsson, B. E., Gutiérrez, E., Hafner, P., Haupt, M., Hilasvuori, E., Heinrich, I., Helle, G., Jalkanen, R., Jungner, H., Kalela-Brundin, M., Kessler, A., Kirchhefer, A., Klesse, S., Krapiec, M., Levanič, T., Leuenberger, M., Linderholm, H. W., McCarroll, D., Masson-Delmotte, V., Pawelczyk, S., Pazdur, A., Planells, O., Pukiene, R., Rinne-Garmston, K. T., Robertson, I., Saracino, A., Saurer, M., Schleser, G. H., Seftigen, K., Siegwolf, R. T. W., Sonninen, E., Stievenard, M., Szychowska-Krapiec, E., Szymaszek, M., Todaro, L., Waterhouse, J. S., Weigl-Kuska, M., Weigt, R. B., Wimmer, R., Woodley, E. J., Vitas, A., Young, G., and Loader, N. J.: Recent human-induced atmospheric drying across Europe unprecedented in the last 400 years, Nat. Geosci., 17, 58–65, https://doi.org/10.1038/s41561-023-01335-8, 2024.

Trouet, V. and Van Oldenborgh, G. J.: KNMI Climate Explorer: A Web-Based Research Tool for High-Resolution Paleoclimatology, Tree-Ring Res., 69, 3–13, https://doi.org/10.3959/1536-1098-69.1.3, 2013.

Vicente-Serrano, S. M., Beguería, S., and López-Moreno, J. I.: A Multiscalar Drought Index Sensitive to Global Warming: The Standardized Precipitation Evapotranspiration Index, J. Clim., 23, 1696–1718, https://doi.org/10.1175/2009JCLI2909.1, 2010a.

Vicente-Serrano, S. M., Beguería, S., López-Moreno, J. I., Angulo, M., and El Kenawy, A.: A New Global 0.5° Gridded Dataset (1901–2006) of a Multiscalar Drought Index: Comparison with Current Drought Index Datasets Based on the Palmer Drought Severity Index, J. Hydrometeorol., 11, 1033–1043, https://doi.org/10.1175/2010JHM1224.1, 2010b.

Wang, W., Zeng, X., Liu, X., An, W., and Zhang, L.: Temporal evolution of the influence of atmospheric circulation on regional cloud cover as revealed by tree-ring $\delta^{18}O$ in southwestern China, Glob. Planet. Change, 208, 103690, https://doi.org/10.1016/j.gloplacha.2021.103690, 2022.

Werner, M., Langebroek, P. M., Carlsen, T., Herold, M., and Lohmann, G.: Stable water isotopes in the ECHAM5 general circulation model: Toward high-resolution isotope modeling on a global scale, J. Geophys. Res., 116, D15109, https://doi.org/10.1029/2011JD015681, 2011.

Wigley, T. M. L., Briffa, K. R., and Jones, P. D.: On the Average Value of Correlated Time Series, with Applications in Dendroclimatology and Hydrometeorology, J. Clim. Appl. Meteorol., 23, 201–213, https://doi.org/10.1175/1520-0450(1984)023%3C0201:OTAVOC%3E2.0.CO;2, 1984.

Xu, C., Sano, M., and Nakatsuka, T.: Tree ring cellulose $\delta^{18}O$ of *Fokienia hodginsii* in northern Laos: A promising proxy to reconstruct ENSO?, J. Geophys. Res.-Atmos., 116, D24109, https://doi.org/10.1029/2011JD016694, 2011.

Xu, C., Sano, M., and Nakatsuka, T.: A 400-year record of hydroclimate variability and local ENSO history in northern Southeast Asia inferred from tree-ring $\delta^{18}O$, Palaeogeogr. Palaeoclimatol. Palaeoecol., 386, 588–598, https://doi.org/10.1016/j.palaeo.2013.06.025, 2013a.

Xu, C., Zheng, H., Nakatsuka, T., and Sano, M.: Oxygen isotope signatures preserved in tree ring

cellulose as a proxy for April–September precipitation in Fujian, the subtropical region of southeast China, J. Geophys. Res.-Atmos., 118, 12805–12815, https://doi.org/10.1002/2013JD019803, 2013b.

Xu, C., Zhao, Q., An, W., Wang, S., Tan, N., Sano, M., Nakatsuka, T., Borhara, K., and Guo, Z.: Tree-ring oxygen isotope across monsoon Asia: Common signal and local influence, Quat. Sci. Rev., 269, 107156, https://doi.org/10.1016/j.quascirev.2021.107156, 2021.

Xu, C., Wang, S.-Y. S., Borhara, K., Buckley, B., Tan, N., Zhao, Y., An, W., Sano, M., Nakatsuka, T., and Guo, Z.: Asian-Australian summer monsoons linkage to ENSO strengthened by global warming, npj Clim. Atmos. Sci., 6, 8, https://doi.org/10.1038/s41612-023-00341-2, 2023.

Xu, C., Huang, R., An, W., Zhao, Q., Zhao, Y., Ren, J., Liu, Y., and Guo, Z.: Tree ring oxygen isotope in Asia, Glob. Planet. Change, 232, 104348, https://doi.org/10.1016/j.gloplacha.2023.104348, 2024.

Zellweger, F., De Frenne, P., Lenoir, J., Vangansbeke, P., Verheyen, K., Bernhardt-Römermann, M., Baeten, L., Hédl, R., Berki, I., Brunet, J., Van Calster, H., Chudomelová, M., Decocq, G., Dirnböck, T., Durak, T., Heinken, T., Jaroszewicz, B., Kopecký, M., Máliš, F., Macek, M., Malicki, M., Naaf, T., Nagel, T. A., Ortmann-Ajkai, A., Petřík, P., Pielech, R., Reczyńska, K., Schmidt, W., Standovár, T., Świerkosz, K., Teleki, B., Vild, O., Wulf, M., and Coomes, D.: Forest microclimate dynamics drive plant responses to warming, Science, 368, 772–775, https://doi.org/10.1126/science.aba6880, 2020.

Zharkov, M. S., Fonti, M. V., Trushkina, T. V., Barinov, V. V., Taynik, A. V., Porter, T. J., Saurer, M., and Churakova (Sidorova), O. V.: Mixed Temperature-Moisture Signal in $\delta^{18}O$ Records of Boreal Conifers from the Permafrost Zone, Atmosphere, 12, 1416, https://doi.org/10.3390/atmos12111416, 2021.

Zolina, O., Simmer, C., Belyaev, K., Kapala, A., and Gulev, S.: Improving Estimates of Heavy and Extreme Precipitation Using Daily Records from European Rain Gauges, J. Hydrometeorol., 10, 701–716, https://doi.org/10.1175/2008JHM1055.1, 2009.